Material characterization of dual-energy computed-tomography data using polar coordinates

Lukas Havla[1], Michael Peller[1], Clemens Cyran[2], Konstantin Nikolaou[2,3], Maximilian Reiser[1,2], Olaf Dietrich[1]

[1] Josef Lissner Laboratory for Biomedical Imaging, Institute for Clinical Radiology, Ludwig-Maximilians-University Hospital Munich, Germany

[2] Institute for Clinical Radiology, Ludwig-Maximilians-University Hospital Munich, Germany

[3] Department of Radiology, University Hospitals Tübingen, Tübingen, Germany.

ELECTRONIC PREPRINT VERSION:
Not for commercial sale or for any systematic external distribution by a third party
Final version: *J Comput Assist Tomogr.* 2015; **39**(1):134–139.
<URL:http://dx.doi.org/10.1097/RCT.0000000000000157 >

Abstract

The purpose of this study was to evaluate a new dual-energy computed-tomography (DECT) post-processing approach based on the transformation of dual-energy radiodensity data into polar coordinates. Given two corresponding DECT images, the attenuation data $D(U_1)$, $D(U_2)$ in Hounsfield units of both tube voltages (U_1,U_2) were transformed for each voxel to polar coordinates: r (distance to the radiodensity coordinate origin) is an approximate measure of electron density and φ (angle to the abscissa) differentiates between materials.

Keywords:
Dual Energy CT, material characterization, contrast agents, experimental investigations, animal studies

Corresponding author:
Lukas Havla
Josef Lissner Laboratory for Biomedical Imaging,
Institute for Clinical Radiology,
Ludwig Maximilians University Hospital Munich,
Marchioninistr. 15, 81377 Munich
(e-mail: lukas.havla@med.uni-muenchen.de).

Introduction

In clinical routine computed tomography (CT), the differentiation between different tissues or materials with equal radiodensity (i. e., exhibiting same Hounsfield unit (HU) values) can be vital for radiologic evaluation and diagnosis. Examples of such materials are blood mixed with iodinated contrast media or tissue matrices containing calcium which, due to varying concentrations of constituent elements, can be indistinguishably similar in radiodensity.

In 1976, Alvarez and Macovski [1] recognized the potential of exploiting the information generated by polychromatic X-ray spectra to improve diagnosis. Avrin et al. [2] investigated the decomposition of projection data into element-specific components, Rutherford et al. [3] showed the possibility to measure the effective atomic number and the clinical relevance was tested by Millner et al. [4]. In utilizing an energy-resolving photon-counting detector, Wang et al. [5] demonstrated the simultaneous separation of more than two types of materials with a single X-ray source. Low-spectral CT can be alternatively achieved by measuring the object simultaneously with two different X-ray tube voltages. Technical limitations of former CT scanners have prevented diagnostic use until 2006, when dual-source CT systems with two independent tube-detector units for the simultaneous acquisition of two X-ray attenuation signals became commercially available. Primarily designed to improve the temporal resolution for rapid cardiac imaging [6,7], the operation of the second X-ray tube with another voltage brought dual-energy CT (DECT) imaging into the clinic [8,9]. Exemplary DECT applications include the assessment of the arteries in the skull base [8], characterization of renal masses [10], or quantification of coronary artery calcium [11].

In the present study, we aimed to demonstrate that materials such as gadolinium or copper in addition to iodine-based contrast materials and calcium-containing structures can be differentiated and characterized by introducing polar coordinates for DECT data post-processing and evaluation.

Materials and Methods

All animal experiments were approved by the institutional animal care and use committee.

Theory

The X-ray linear attenuation coefficient μ is correlated to the energy E of the photon, the atomic number Z of the interacting matter, and material concentration C. The Hounsfield unit scale is a quantitative measure for the radiodensity D of a given material:

$$D = \frac{\mu_{\text{material}} - \mu_{\text{water}}}{\mu_{\text{water}}} \times 1000 \quad \text{HU} \tag{1}$$

related to the linear attenuation coefficients μ of the material and of water as reference. In DECT, two image datasets, $D_{(x,y,z)}(U_1)$ and $D_{(x,y,z)}(U_2)$, (where (x,y,z) denotes the spatial voxel position) are simultaneously acquired with element-specific radiodensities depending on the two different tube voltages $U_1 > U_2$. Typically, these two datasets are either evaluated separately, or used to calculate derived datasets such as one corresponding to an intermediate tube voltage or to a virtual non-contrast acquisition [8,12].

The energy (or tube voltage) dependence of the radiodensity datasets can be displayed in a dual-energy plot [6] where both tube voltages are plotted on horizontal and vertical axis, respectively.

To improve and simplify the analysis of two or more materials at the same time, we propose a non-linear coordinate transformation of the data shown in the scatter plot from Cartesian radiodensity coordinates $(D_{(x,y,z)}(U_1), D_{(x,y,z)}(U_2))$ into polar coordinates $(r_{(x,y,z)}, \varphi_{(x,y,z)})$ by the following standard relation:

$$r_{(x,y,z)}(U_1, U_2) = \sqrt{D_{(x,y,z)}(U_1)^2 + D_{(x,y,z)}(U_2)^2} \tag{2}$$

$$\varphi_{(x,y,z)}(U_1, U_2) = \operatorname{atan}2\left(D_{(x,y,z)}(U_2),\ D_{(x,y,z)}(U_1)\right) \tag{3}$$

with $r_{(x,y,z)} \geq 0$ and $-\pi < \varphi_{(x,y,z)} \leq \pi$. The function $\operatorname{atan}2(a_1, a_2)$ is defined as the arctangent function with two arguments (a_1, a_2) frequently used in computer programming languages such as FORTRAN. We assign the first argument to the lower DECT voltage U_2 (80 kV or 100 kV) and the second argument to the higher voltage U_1 (140 kV).

Phantom Setup

For experimental validation, we prepared a phantom consisting of 10 vials. Used chemical substances were: 1) gadobutrol (Bayer Vital, Leverkusen, Germany) containing gadolinium (Gd) in 3 different dilutions, 2) iomeprol (Bracco Imaging, Konstanz, Germany) containing iodine (I), also 3 dilutions, 3) copper (II) sulfate, diluted from

min. 99% (Sigma-Aldrich, Saint Louis, MO, USA) containing copper (Cu), 4) rod material coming with Gammex Phantom 467 (Gammex, Middleton, WI, USA) containing calcium (Ca), and as reference 5) H_2O. The arrangement of vials and the different dilutions are shown in table 1.

Animal model

In vivo data of 10 female athymic rats (7-8 weeks old, Harlan Laboratories Inc., Indianapolis, IN, USA) were taken retrospectively from another study approved by the Government of Upper Bavaria Committee for Animal Research (Gz.55.2-1-54-2532-33-10) and carried out in accordance with the guidelines of the National Institute of Health for the care and use of laboratory animals.

Scanning Protocol and Radiation Dose

The phantom was imaged in a DECT scanner (SOMATOM Definition Flash, Siemens Healthcare, Forchheim, Germany) equipped with two independently operating X-ray tube and detector units. Two protocols were used:
(1) tube voltage U_1=80 kV (tube current-time product: 650 mAs) and tube voltage U_2=140 kV (251 mAs) with 1 mm tin filter, denoted as 140 kV_{Sn};
(2) U_1=100 kV (650 mAs) and U_2=140 kV_{Sn} (502 mAs). The first sequence yielded CTDIvol (L=32 cm) of 24.35 mGy and the second one CTDIvol of 50.09 mGy. The reconstruction matrix size was 512×512×8 with a diameter of 406 mm and a slab thickness of 16 mm. Two quantitative kernels (D20s and D40s) were used for image reconstruction in order to assess their influence on the polar-coordinate transformation.

In vivo DECT perfusion images were acquired over 90 seconds (temporal resolution: 1 s) with tube voltages U_1=80 kV (200 mAs) and U_2=140 kV_{Sn} (78 mAs); 2 mL/kg bodyweight of iopromide (Ultravist 370®, Bayer HealthCare, Berlin, Germany) were injected.

Post-Processing and Statistical Analysis

We used in-house-developed software programmed in IDL (v8.2.2; Exelis Visual Information Solutions Inc., Boulder, CO,USA) to transform the two reconstructed DECT phantom image datasets, $D_{(x,y,z)}(U_1)$ and $D_{(x,y,z)}(U_2)$, into polar-coordinate data sets, $r_{(x,y,z)}(U_1,U_2)$ and $\varphi_{(x,y,z)}(U_1,U_2)$. Rectangular regions of interest (ROI) of each vial containing 391 voxels in each slice were selected yielding a total of 3128 voxels. ROI data of radiodensities of both voltages (in HU) and their corresponding polar parameter maps (r,φ) of both kernels were included in the analysis.

Data were statistically evaluated using R (v3.0.1; R Foundation for Statistical Computing, Vienna, Austria). To assess the feasibility of the polar angle, φ, for material discrimination, ROI values from samples containing the same basis material, but at different concentrations, were pooled together. Box-and-whisker plots and histograms were computed of the polar-angle distribution.

For evaluation of the influence of the material concentration on the polar radius, r, all ROIs were evaluated separately; Pearson correlation coefficients for the probes containing I, Gd, and Ca as well as linear regression lines were calculated using the H_2O sample as zero-concentration sample for all materials.

In vivo data were also transformed to φ and r maps as described above. In each dataset, two ROIs were drawn in a large vessel and in the vertebral column, representing iodine and calcium. The iodine ROI was defined in two subsequent arterial phases of one slice of the 80-kV dataset by selecting all voxels with values ranging from 2000 to 3000 HU. The calcium ROIs were manually placed in a vertebral body in one slice and one dynamic phase. The polar angle φ was averaged in each ROI; mean values and standard deviations were determined over all animals.

Results

An exemplary rat dataset was used for illustration in figure 1. In this scatter plot the radiodensities $D_{(x,y,z)}(U_1)$ and $D_{(x,y,z)}(U_2)$ of datasets containing soft tissue, bone and iodine are plotted along the horizontal and the vertical axis, respectively [6]. Due to element-specific attenuation properties, distributions of both iodine and calcium are nearly linear yet distinctly separate.

Table 1. For the phantom experiment chemical substances (molar concentration in mol/L), rod material (ρ_e^w : electron density relative to water) from Gammex phantom plus H_2O as reference are examined (alignment according to phantom in figure 2).

Phantom	column 1	column 2	column 3	column 4
row 1	**Iomeprol (I1)** 0.064 mol/L	**Iomeprol (I2)** 0.032 mol/L	**Iomeprol (I3)** 0.016 mol/L	
row 2	**Gadobutrol (Gd1)** 0.3 mol/L	**Gadobutrol (Gd2)** 0.2 mol/L	**Gadobutrol (Gd3)** 0.1 mol/L	
row 3	**$CuSO_4$ (Cu1)** 1.253 mol/L	**Cortical Bone (Ca1)** ρ_e^w =1.69	**CB2 50% (Ca2)** ρ_e^w =1.47	**H_2O**

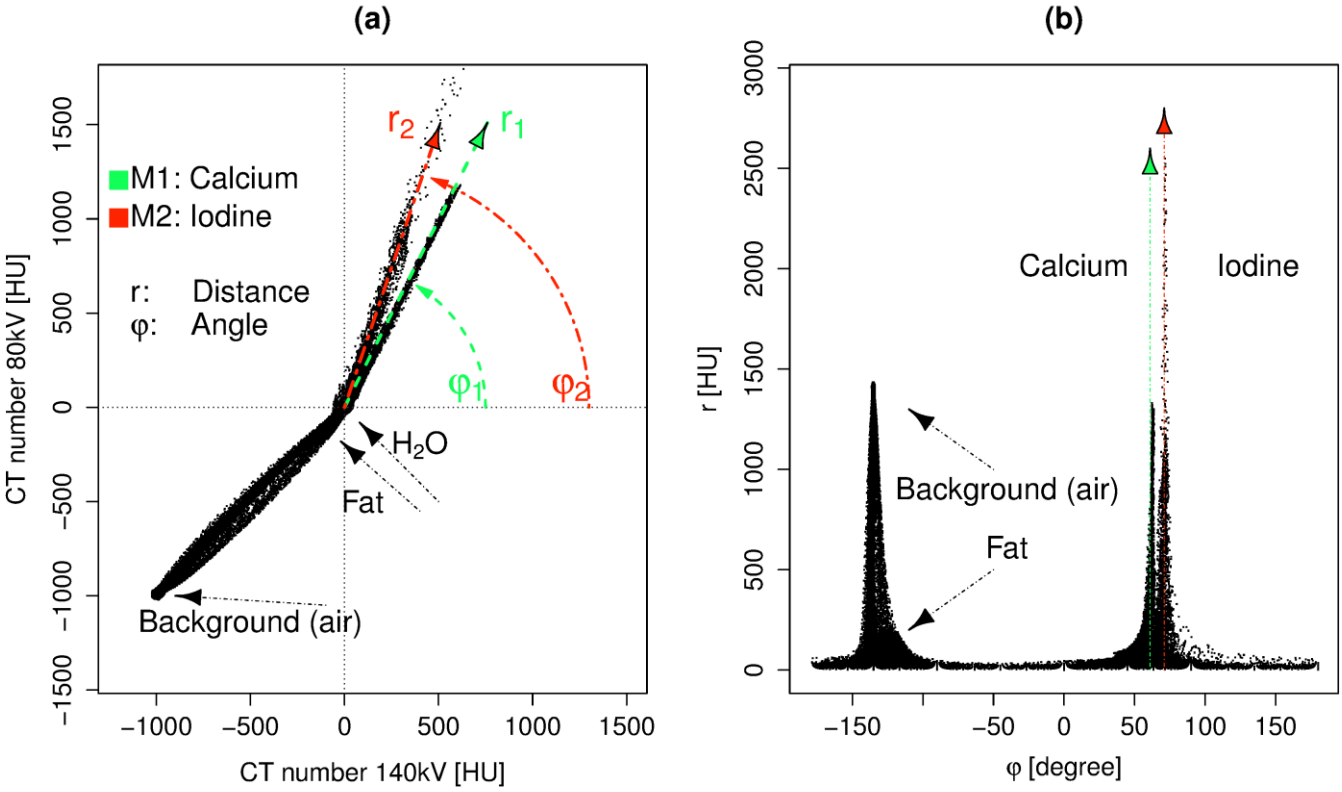

Figure 1. (a): Illustration of a typical in vivo Dual Energy CT (DECT) dataset in Cartesian coordinates as voxel-by-voxel scatterplot. Dashed lines show polar properties of two different materials M1 (calcium) and M2 (iodine). A change in concentration of any material approximately does not affect the angle φ but only *r*. (b) shows the φ - r scatter plot after polar-coordinate transformation of the same dataset.

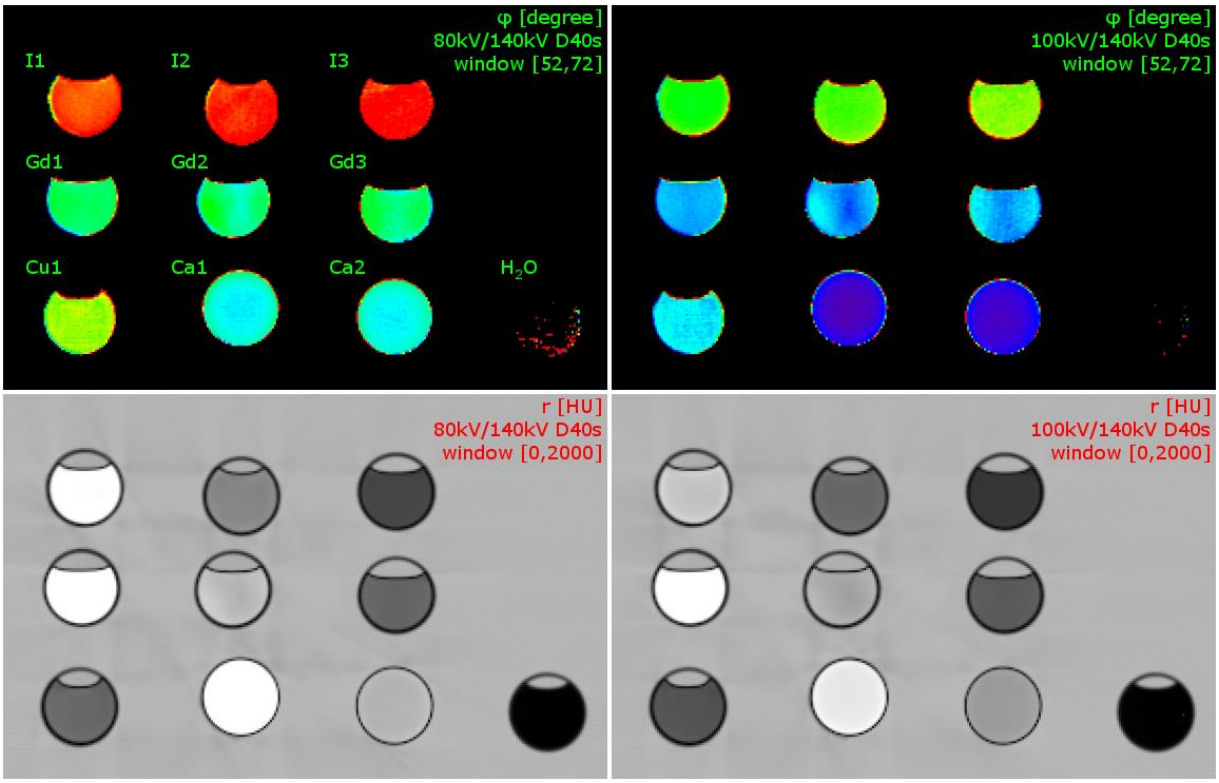

Figure 2. Polar parameter maps of the entire phantom reconstructed with D40s convolution kernel. Left column: tube-voltage pair 80 kV/140 kVSn; right column: 100 kV/140 kVSn. The top row shows the parameter map φ, the bottom one the parameter r. Window setting is chosen to give optimal contrast [<low>,<high>].

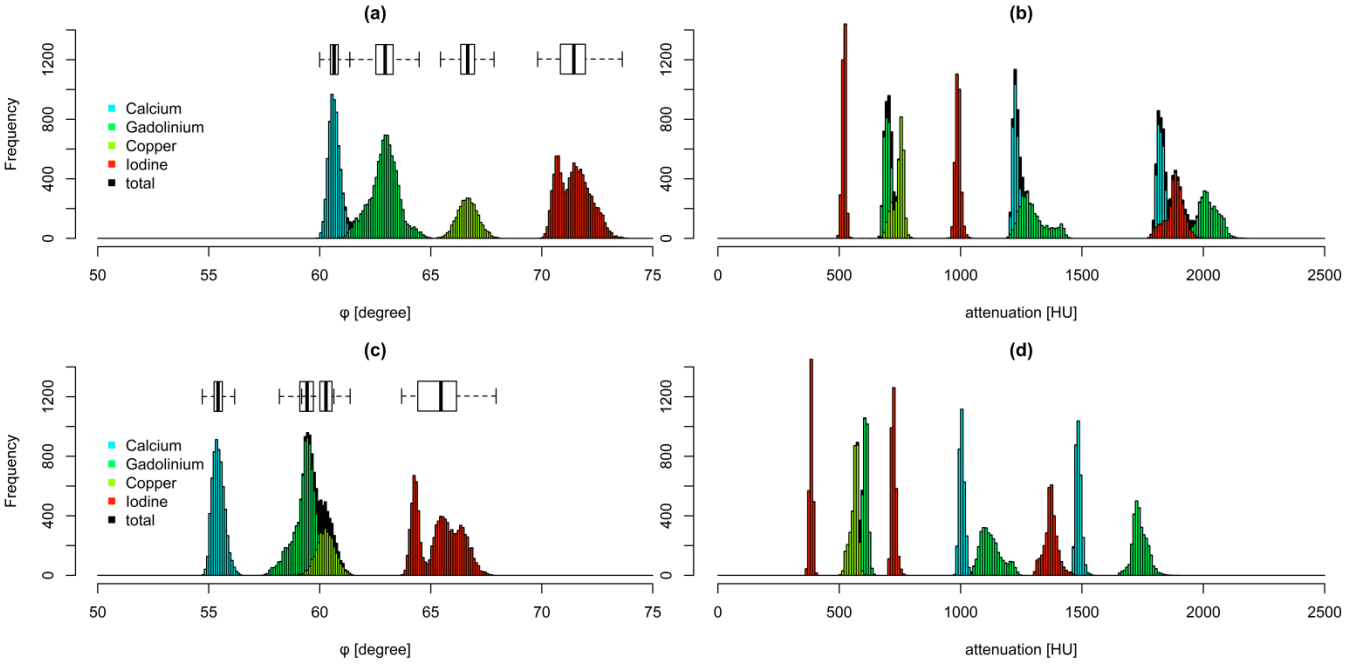

Figure 3. Histograms and box-and-whisker plots for both tube-voltage pairs. The upper row (a,b) shows the combination of 80 kV/140 kV_{Sn}, the lower one (c,d) 100 kV/140 kV_{Sn}. The left column (a,c) contains the boxplots and histograms of the polar angle φ and the right one (b,d) the histogram of the lower-voltage (80 kV or 100 kV, respectively) HU data.

Table 2. Statistical analysis of parameter φ regarding both reconstruction kernels. Pixel values of single probes and rods of different materials are taken together and following parameters are calculated: mean and standard deviation. Furthermore the absolute differences are displayed between kernels D40s and D20s.

φ [degree]		80 kV				100 kV			
		Ca	Gd	Cu	I	Ca	Gd	Cu	I
D40s	mean	60.67	62.90	66.66	71.47	55.44	59.40	60.27	65.39
	std	0.26	0.65	0.46	0.71	0.27	0.59	0.41	0.92
D20s	mean	60.67	62.90	66.66	71.47	55.44	59.39	60.27	65.39
	std	0.23	0.62	0.36	0.67	0.25	0.56	0.32	0.90
difference	mean	-0.0022	0.0034	0.0017	0.0002	-0.0013	0.0017	0.0024	0.0004
	std	0.0396	0.0313	0.1050	0.0393	0.0238	0.0221	0.0958	0.0236

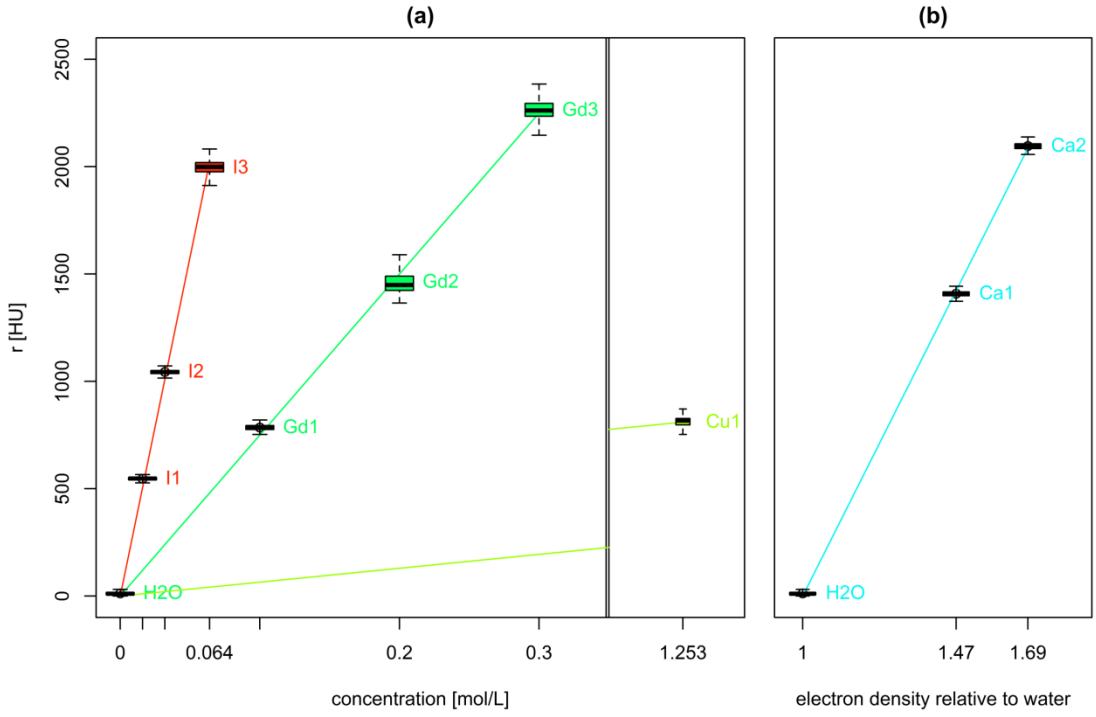

Figure 4. Plot of parameter *r* over concentration and electron density. Box-and-whisker plots superimposed by linear regression lines through iodine, gadolinium, copper, and calcium samples plus H_2O are shown. The parameter *r* is a linear measure for the concentration of the examined substance.

Maps of the polar parameters φ (color-coded) and *r* (gray-scaled) of the phantom measurements with both protocols (reconstruction kernel D40s) are displayed in figure 2. As illustrated by the different colors, φ provides a good discrimination of the kind of material examined, whereas the parameter *r* is a measure for the concentration.

Figure 3 shows the acquired data of 9 samples (without H_2O) from 80 kV/140 kV_{Sn} and 100 kV/140 kV_{Sn} scans reconstructed with the D40s convolution kernel as histograms. At both energy pairs, different characteristic angles φ for all four substances can be observed in subplots (a) and (c).

In contrast, the histograms of the conventional HU values (here from the low-kV dataset) show an ambiguous distribution over the HU range (figures 3(b) and 3(d)) with clear influence of the varying concentrations. The box-and-whisker plots boxes above the histograms (figures 3 (a), 3(c)) indicate that the dispersion is small relative to the distance of the peaks. The non-paired, two-sided t-test revealed significant differences ($p<0.0001$) between all materials at both energy pairs (independent of the applied reconstruction kernel).

Comparing figure 3(a) and figure 3(c), it can be observed that the element-specific polar angle

depends on the tube-voltage pair used for the experiment; increasing the lower tube voltage from 80 to 100 kV results in a global shift of approximately –5° on the φ-axis. Furthermore, between 80 kV/140 kV_{Sn} and 100 kV/140 kV_{Sn}, the pattern of the angle distribution changes considerably, in particular, the φ peaks of copper and gadolinium start to overlap in the 100 kV/140 kV_{Sn} data.

Regardless of a doubled radiation dose when acquiring 100 kV/140 kV_{Sn} data, the standard deviation (i. e., the width of the peaks) remains approximately the same.

A comparison of the parameter φ reconstructed with kernels D40s and D20s shows that mean values of the parameter φ differ less than 0.01° for all materials at both tube-voltage pairs and the standard deviation difference is in the range between 0.01° and 0.1° (table 2).

In figure 4, the relationship between the radial polar parameter r and the concentration of the examined material is presented. The results illustrate that r depends approximately linearly on the concentration (slope coefficients in [HU/(mol/L)] are 31,584, 7,499, and 647 for iodine, gadolinium, and cupper, respectively). The Pearson's correlation value of mean values for iodine, gadolinium, and calcium and their concentrations are 0.9996 (p-value<0.001), 0.9995 (p<0.001), and 0.9999 (p<0.01).

In vivo measurements yielded mean polar angles φ of 62.9°±0.4 (range 62.3° to 63.4°) for the calcium ROI and of 71.6°±0.3 (range 71.2° to 72.0°) for the iodine ROI.

Discussion

The use of polar coordinates introduces a new visualization method of dual energy data. The implementation is mathematically and computationally simple. This DECT study was performed to demonstrate the application of polar coordinates in phantom data and in vivo to analyze and visualize the material dependence of the energy-specific linear attenuation coefficients.

Using materials such as Ca, Gd, Cu, and I, we illustrated that each of these materials can be differentiated based on the polar angle φ derived from the scatter plot of energy-dependent attenuations (figure 2 and 3). In vivo data shows high interindividual reproducibility and good agreement with the phantom data (acquired at the same tube voltages) with absolute differences of element-specific φ values of 0.1° for iodine and 2.2° for calcium. One reason for the divergent results is the slightly different chemical composition of the rat backbone vs. calcium carbonate which was used in the phantom.

The radial parameter r (being the quadratic mean of the two individual DECT radiodensities) is proportional to the concentration of the material (figure 4) with excellent correlation coefficient greater than 0.999.

The presented histogram data (figure 3) shows that the element-specific φ values depend on the applied tube-voltage pair. All four examined materials (Ca, Gd, Cu, I) can be discriminated at both tube-voltage pairs. Overall, the 80 kV/140 kV_{Sn} tube voltage pair provides better separation of the element-specific energy spectra. Overlap reduces the specificity (or uniqueness) of dual-energy information and results in divergent angles (iodine shows two peaks). Therefore, better spectral separation for material discrimination is required.

Dual-energy data exhibits radial behavior depending on the material (c.f. DE scatter plot in figure 1(a)) because the Hounsfield unit scale defines water (0 HU) as point of origin independent of the applied tube voltage. Therefore the application of the polar-coordinate transformation is naturally motivated.

In 2009 Primak et al. [13] showed the importance of optimized spectral filtration on dual energy material discrimination. In simulation and phantom experiments the spectral separation was increased (and overlap decreased, respectively) by selecting proper filter materials at appropriate thicknesses. In their study they introduced the "dual-energy ratio" DE_{ratio}, which is defined as the quotient of the slopes calculated for low (U_2)- and high (U_1)-energy CT numbers at different concentrations of a certain material. They conclude that the difference in the DE_{ratio} determines the contrast between two materials proposing optimal spectral filtration.

In contrast to our proposed method, the discrimination of materials by displaying the DE_{ratio} is conceptually less clear because the material concentration is either lost or must be derived by calculating the distance from the pole, i. e., by (half a) polar-coordinate transformation. Polar

coordinates, thus, reduces complexity because kind of matter is defined by the angle and concentration by the radial component. In addition, the irregular behavior of the DE_{ratio} with very large (approximately infinite) slopes for small voltages is avoided by polar coordinates. New technical advances will improve photon output at voltages of 80 kV and lower resulting in yet better spectral separation. Thereby the contrast between the low-kV and high-kV dataset is maximized and the DE slope approaches infinity. Finally, DE_{ratio} is not unique if organs such as lung tissue or other materials with CT numbers lower than 0 HU are assessed. For the application of polar-coordinate transformation it is not required to adapt DECT scan parameters or increase the radiation dose. Quite the contrary: our results indicate that better tissue discrimination depends solely on the separation of the X-ray spectra rather and not on increasing the time-current product and hence radiation dose: 80 kV/140 kV_{Sn} data outperform the other one despite approximately doubled radiation dose with regard to the polar parameter φ.

The theoretical quantitative calculation of the polar angle φ is complex: It depends to some extent on the atomic number Z, but not in a monotonic way, since the angle increases from Ca (Z=20), over Gd (Z=64) and Cu (Z=29) to I (Z=53). Considering the details of the X-ray spectra for different tube voltages, spectral filtration, the mass attenuation coefficients for the examined elements, and, in particular, the corresponding atomic absorption edges, the physical analysis was beyond the scope of this work.

The precision of the determined polar angle φ increases with the associated radius r; i. e., more precise values of φ can be expected for materials with high attenuation than for materials with HU values close to zero (such as water or soft tissue). Further studies are required to investigate the value of the angle φ in the low-concentration range (from –1000 HU to 0 HU), e. g., to distinguish foams of different materials.

In conclusion, the application of the polar-coordinate transformation to DECT data allows to uniquely characterize and differentiate elements like calcium (present in bone or calcified tissues) and iodine or gadolinium contrast agents based on their specific polar angle φ. Correspondingly, the distance r is an approximate measurement of electron density. In our study we could show feasibility and parameter reproducibility in vivo and in vitro. Better performance can be expected with the upcoming advances in X-ray tube design and with the development of brilliant mono-energetic X-ray photon sources as well as with improvements on the detector site.

References

1. Alvarez RE, Macovski A. Energy-selective reconstructions in X-ray computerised tomography. *Phys. Med. Biol.* 1976;21:733–744.

2. Avrin DE, Macovski A, Zatz LE. Clinical application of Compton and photo-electric reconstruction in computed tomography: preliminary results. *Invest. Radiol.* 1978;13:217–22.

3. Rutherford RA, Pullan BR, Isherwood I. X-ray energies for effective atomic number determination. *Neuroradiology*. 1976;11:23–8.

4. Millner MR, McDavid WD, Waggener RG, et al. Extraction of information from CT scans at different energies. *Med. Phys.* 1979;6:70–1.

5. Wang X, Meier D, Taguchi K, et al. Material separation in x-ray CT with energy resolved photon-counting detectors. *Med. Phys.* 2011;38:1534.

6. Flohr TG, McCollough CH, Bruder H, et al. First performance evaluation of a dual-source CT (DSCT) system. *Eur. Radiol.* 2006;16:256–68.

7. Johnson TRC, Nikolaou K, Wintersperger BJ, et al. Dual-source CT cardiac imaging: initial experience. *Eur. Radiol.* 2006;16:1409–15.

8. Johnson TRC, Krauss B, Sedlmair M, et al. Material differentiation by dual energy CT: initial experience. *Eur. Radiol.* 2007;17:1510–7.

9. Graser A, Johnson TRC, Chandarana H, et al. Dual energy CT: preliminary observations and potential clinical applications in the abdomen. *Eur. Radiol.* 2009;19:13–23.

10. Brown CL, Hartman RP, Dzyubak OP, et al. Dual-energy CT iodine overlay technique for characterization of renal masses as cyst or solid: a phantom feasibility study. *Eur. Radiol.* 2009;19:1289–95.

11. Schwarz F, Nance JW, Ruzsics B, et al. Quantification of coronary artery calcium on the basis of dual-energy coronary CT angiography. *Radiology*. 2012;264:700–7.

12. Graser A, Johnson TRC, Bader M, et al. Dual energy CT characterization of urinary calculi: initial in vitro and clinical experience. *Invest. Radiol.* 2008;43:112–9.

13. Primak AN, Ramirez Giraldo JC, Liu X, et al. Improved dual-energy material discrimination for dual-source CT by means of additional spectral filtration. *Med. Phys.* 2009;36:1359.